AZIMUTHAL OFFSET-DEPENDENT ATTRIBUTES (AVO AND FVO) APPLIED TO FRACTURE DETECTION

Feng Shen, Jesus Sierra, Daniel R. Burns, and M. Nafi Toksöz

Earth Resources Laboratory
Department of Earth, Atmospheric, and Planetary Sciences
Massachusetts Institute of Technology
Cambridge, MA 02139

ABSTRACT

Using the amplitude versus offset (AVO) and the frequency versus offset (FVO) information, the diagnostic ability of P-wave seismic data in fracture detection is investigated. The offset-dependent attributes (AVO and FVO) are estimated by using an eigenvector based estimation technique, the multiple signal classification frequency estimator. These attributes are applied to the determination of principal orientation of fractures in carbonate fractured reservoirs located in the Maporal field in the Barinas basin of southwestern Venezuela. Our studies show that, in the crack normal direction, P-wave reflectivity is characterized by a large increase of amplitude with offset (large positive AVO gradient) and a large frequency decay with offset (large negative FVO gradient). In the crack strike direction, P-wave reflectivity is characterized by a wide range of AVO gradients but a small variation of FVO gradients. The analyses of inverted offset-dependent velocities and theoretical calculations show that the lateral heterogeneity in the reservoir zone can lead to large variations of AVO signatures. The offset-dependent frequency attribute can help lessen the ambiguity in fracture detection. The combination of the offset-dependent frequency attribute is more beneficial than using the offset-dependent amplitude attribute alone.

INTRODUCTION

With advanced horizontal drilling technology, determining fracture orientation is very important. Well log data can be used for fracture detection but are limited to well locations. Geologic observations can be used to predict fracture orientation but only

with certain assumptions. Seismic data have wider spatial coverage than well data, and thus fracture estimation from seismic data becomes important for practicality. It is known that vertically aligned fractures in a reservoir induce seismic anisotropy. Shear wave splitting can be observable in fractured reservoirs and is very sensitive to the fracture orientation and density. However, high acquisition cost of multicomponent data makes this method expensive to apply on a regular basin. In addition, processing of multicomponent data requires technology that the seismic industry has not yet fully developed. Using P-wave data to detect fractures is very promising and has been of growing interest to the exploration geophysical community recently.

Studies show that the effect of vertically aligned fractures on P-wave reflectivity is a function of offset and cannot be detected by conventional normal incident seismic data. For this reason, fracture studies based on seismic data analysis have been extended to prestacked seismic data. Determining the principal orientations of vertically aligned fractures from P-wave data presently depends on velocity analysis studies for different common midpoint (CMP) locations and on AVO studies for different azimuthal angles. Neidell and Cook (1986) use the differential informational stacking velocity analysis method to identify subsurface fracture zones from P-wave data. They claim that anomalous velocity zones are related to fractures. Paul (1993) attributes anomalously low stacking velocities to the presence of localized fractures. The similar phenomenon of stacking velocity anomalies induced by fractures is observed by Lynn *et al.* (1995) and Corrigan *et al.* (1996). If the fracture layer has a small thickness, the application of P-wave stacking velocity is limited because the azimuthal travel time depends on both the fracture parameters and the thickness of the fractured reservoir. Unlike stacking velocity analysis methods, azimuthal AVO studies, relying on the reflection amplitudes, have been used to detect fractures (Perez and Gibson, 1996; Ramos and Davis, 1997; Mallick *et al.*, 1998).

Generally, amplitudes are related to reflection coefficients and thus to elastic contrasts across the reflection boundary. The predication of fracture orientation based on azimuthal variations is still ambiguous when *a priori* knowledge of some variables, such as layer thickness and spatial heterogeneity caused by fluid content and lithology, are not available. Therefore, other seismic parameters, in addition to AVO, are needed to reduce the ambiguities and constrain solutions in the interpretation of fractured reservoirs. Finding additional parameters appears to be feasible in prestacked domains because the seismic signal can be parameterized in terms of amplitude, phase and frequency versus offset. Mazzotti (1991) applies instantaneous amplitude, phase and frequency versus offset (APF.VO) indicators to investigate the possibility of a diagnostic value of seismic data and shows that modifying the velocities and thicknesses of a given target layer, by introducing different pore fluids or lithological conditions, produces changes in instantaneous APF.VO plots in synthetic seismograms. Moreover, Mazzotti (1991) finds that the amplitude indicator appears to be reasonably stable while the phase indicator has a higher spatial variability and a stronger sensitivity to noise.

Based on a 3-D finite difference modeling technique, studies in heterogeneously frac-

tured reservoirs show that, in addition to the azimuthal AVO variations, frequencies of power spectral peaks (signal frequencies) in the crack normal direction shift toward a lower frequency range than those in the crack strike direction. Moreover, at the top of fractured reservoirs, the characteristic of frequency versus offset (FVO) is dominated by the mean of fracture density (Shen and Toksoz, 1998).

In this paper, we demonstrate the application of AVO and FVO analyses to the detection of the principal orientation of fractures from P-wave seismic data in the Maporal field in the Barinas Basin of southwestern Venezuela. Our seismic data analysis consists of studying seismic trace morphology and estimating offset-dependent attributes by using a frequency estimator in three seismic survey lines. We relate these offset dependent attributes to fracture properties and analyze their lateral variations. By combining offset-dependent velocity analyses with theoretical calculations, we investigate the effects of reservoir properties on AVO signatures. Our purpose in this study is to show that, in fracture detection, the combination of offset-dependent frequency attribute is more beneficial than using the offset-dependent amplitude attribute alone.

SEISMIC FIELD DATA

The Maporal field is located in the Barinas Basin, in the southwestern part of Venezuela. Two-dimensional, three-component seismic data were acquired in this field. Three 10 km seismic lines are centered over the areas of interest and cover three azimuths. There are two systems of normal faults: one runs northeast-southwest and the other northwest-southeast. The geometry of seismic lines and well log locations is shown in Figure 1. The azimuths of line 3 and line 1 are almost parallel to the northwest-southeast and northeast-southwest fault systems, respectively; the third line (line 2) almost bisects them and forms an angle of approximately 40° with line 1. A charge of one kilogram explosives at 10 m depth was used for the source. The shotpoint space intervals are 51 m, and the source offset is 17 m. The near offset is 17 m and the far offset can extend to about 3600 m. The maximum fold is 33 traces. The detailed survey parameters can be found in Ata and Michelena (Table 2, 1995).

Like acquisition operations, processing operations also play an important role in seismic data quality control. Our processing sequence aims to remove the distorting effects partially caused by ground coupling of sources and receivers, source-receiver patterns and near surface conditions, to increase the signal to noise ratio and to preserve true amplitudes. We avoid adaptive processes such as signal-trace deconvolution, spectral whitening and amplitude scaling. The processing sequence applied to the three lines includes true amplitude recovery, F-K filter, refraction statics, CMP sorting, normal moveout (NMO) and residual statics. This sequence is summarized in Figure 2. After a two-passes velocity analysis, trace editing and bandpass filtering are performed. The reflection amplitudes are not biased by processing algorithms, so the amplitudes can be used to obtain offset-dependent seismic attributes to characterize fractured reservoirs. Considering that reservoirs are near the intersection point of the three lines and that

azimuthal comparison of offset-dependent attributes are conveniently made, a subset of data is selected from the whole data set for this study. Sixty CDPs in each line are used in our attribute estimation from CDP 221 to CDP 280. The three lines intersect each other around CDP 224.

The reservoir is in the member 'O' of the upper Cretaceous Escandalosa formation at a depth of approximately 3000 m. It consists of dolomitic carbonate and carbonate that contains primary fractures, revealed by televiewer logs. Member 'O' overlays members 'P' and 'R', which are composed mainly of sandstones and shales. To locate the target zone in the seismic profile, synthetic seismograms are generated by using sonic logs from wells that intersect or are close to these lines. The wavelet is extracted from the well logs. Figure 3 shows the synthetic seismograms generated from Well 13 and tied with the stacked P-wave section of line 1. The fractured limestone reservoir is around 2320 ms in seismic profiles and characterized by strong reflectivity.

ESTIMATION OF OFFSET-DEPENDENT ATTRIBUTES

Effects of Tuning and Trace Morphology on Attribute Estimation

On average, the P-wave seismic data have a peak frequency around 25 Hz at the reservoir zone. Using an interval velocity of about 5150 m/s, the corresponding tuning thickness is 39.6 m (with the thickness = $\lambda/5.2$, where λ is the wavelength of the seismic pulse at the peak frequency), or 15 ms in terms of travel time). The thickness of member 'O' does not vary greatly over the research CDP range (60 CDPs, 1.06km), averaging 30 m (12 ms in terms of travel time). Studies from Ramos and Davis (1997) show that tuning has an important effect on the magnitude of AVO gradients and that varying the thickness of a reservoir can lead to variations of AVO gradients when the maximum thickness is smaller than half a wavelength. To investigate the distortion of tuning on azimuthal variations of AVO and FVO, we use the same background model parameters as in previous studies (Shen and Toksoz, 1998) and decrease the thickness of the fractured reservoir to within $\lambda/4$. We find that tuning distorts AVO and FVO properties in fractured reservoirs in the crack normal and strike directions. However, the azimuthal variations of AVO are still observable and FVO gradient in the crack normal direction is still greater than that of the crack strike direction. Considering that the variations in the thickness of the reservoirs are small in our research area, the tuning effect should be similar for most of the data in our analysis, i.e., the tuning effect should produce similar changes in the magnitude of the AVO gradient in the three lines. The azimuthal variations of seismic attributes are still valid in detecting the principal orientation of fractures.

The prestacked CDP gathers in the reservoir target zone are characterized by increasing amplitudes from the near offset to the far offset. Anisotropic surface resolution arises from the oblique incident angles and leads to high resolution in near to middle offset traces and low resolution in far-offset traces. The spatial resolution variation can be explained by the fact that an impinging planar wave has maximum spatial resolving power in the direction of the propagation and no resolving power in the perpendicular

direction. In between the two directions, the resolving power drops off as the cosine of the incident angle (Levin, 1998). Therefore, a real stretch is contained in nonzero offset data. However, for data with similar offset ranges, the stretch is approximately equal. The azimuthal variations of seismic attributes are still valid in detecting the principal orientation of fractures when the spatial stretch is considered.

Additionally, reflection seismic waveforms in the near to middle offset are different from those in the far offset in trace morphology and show large variations in amplitudes, lateral continuity, total energy and energy distributions. Based on the characteristics of CDP gathers in trace morphology, we classify CDP gathers in the three seismic survey lines into two groups: near-middle offset and far offset. The average far offset range for the three lines is from 2000 to 3550 m. CDP gathers with different characteristics in seismic morphology from CDP 245 to CDP 249 in the three lines are shown in Figure 4. It can be found from Figure 4 that far-offset data in CDP gathers are more stable and have smaller lateral variations in seismic morphology than these near-middle offset amplitudes. Additionally, reflectivity in the far offset are characterized by large amplitudes and smooth variations with the offset.

Partial stack amplitudes over near-middle offset data are generated on the NMO corrected gathers (denoted as near-middle poststack amplitudes). Poststack amplitudes with far-offset data and with a full range of offset data are also generated (denoted as far-offset poststack amplitudes and overall poststack amplitudes). These three kinds of stacked seismic profiles are shown in Figure 5. The characteristics of far offset, poststack amplitudes in line 1, line 2 and line 3 are comparable with those of overall poststack amplitudes. This comparability indicates that the contribution of far offset amplitudes to overall poststack amplitudes is greater than that of near-middle offset amplitudes and that far-offset amplitudes dominate the properties of overall poststack amplitudes. Moreover, near-offset amplitudes are most related to reservoir P-wave lithological properties, while far-offset amplitudes contain Poisson's ratio or Vp/Vs information. In fractured reservoirs, the effects of fractures on reflection amplitudes in off fracture strike directions increase with increasing offset. Far offset reflection data contain more information about fractures than near-middle offset data. Therefore, offset dependent attributes estimated from seismic waveforms with approximately equal far offset ranges are still valid in detecting fractures.

Estimation of AVO and FVO Attributes

In CDP gathers, far-offset traces are more stable and have smaller lateral variations in seismic morphology than those of near-middle offset. To avoid errors caused by rapid lateral morphology variations in near-middle offset traces and errors caused by interference among reflection layers, classified far offset seismic waveforms are used to estimate offset-dependent attributes instead of seismic waveforms with a full range of offset. Another advantage of using far offset seismic waveforms in our estimation is that robust offset-dependent attributes, AVO and FVO gradients, can be obtained from fitting with the straight line. Therefore, the bias due to a rapid increase in amplitudes

between the near-middle and far offset can be avoided.

The length of the time window corresponding to the reservoir depth interval has little variation in the far-offset range. We analyze the CDP gathers in a constant time window of 40 ms, starting from the top of the reservoir trough and including 21 samples. Seismic attributes used to determinate fracture orientation are estimated from these waveforms within the time window length. The measured seismic waveforms at the time window of the reservoir zone actually correspond to an averaged medium composed of carbonates and interbedded non-carbonate materials (typically shales) and sands from the member 'P' beneath the member 'O'.

We apply a technique—the multiple signal classification method—to extract AVO and FVO attributes in the frequency domain. This method is based on an eigenanalysis of an autocorrelation matrix and separates information in the autocorrelation matrix into two vector subspaces, one a signal space and the other a noise space. Functions of the vector in either the signal or noise space can be used to create frequency estimators. The power spectral peak values estimated by the frequency estimator represent the strength of the signals. The signal locations in the frequency range indicate the signal frequencies. Note that the frequency estimator is a pseudo spectrum estimator because the autocorrelation sequence cannot be recovered by Fourier transforming the frequency estimator. A detailed discussion about the frequency estimator can be found in Schmidt (1986) and Johnson and Degraaf (1982). This method also has been used in fracture scattering studies and discussed in Shen and Toksöz (1998).

Figure 6 shows that the normalized P-wave power spectra and their frequencies for the reflection at the fractured reservoir zone as a function of offset, corresponding to the CDPs shown in Figure 4 for the three lines. A linear regression, based on the criterion of the least absolute deviations, is used to obtain gradients of amplitudes (power spectra) and frequencies with offset. Because we are interested in the variations of amplitudes with offset, the P-wave amplitudes (power spectra) of each CDP are normalized by the amplitude (spectrum) with the smallest offset. This normalization does not affect the comparative analysis in azimuth. The obtained AVO estimates are relative values and do not correspond to direct measurements of rock properties.

AZIMUTHAL AVO AND FVO ANALYSES

Frequency-dependent (AVO and FVO) attributes are estimated from a total of 180 CDPs in three lines and show specific characteristics. The distributions of the CDPs of three lines in attribute space are shown in Figure 7a. The CDPs, not being overlaid, in three lines show their own specific characteristics which separate them in attribute space. CDPs with the red star in line 1 are characterized by a large increase in amplitude with offset and a large frequency decay with offset. In our estimation, large positive AVO gradients and large negative FVO gradients obviously distribute between CDP 235 and CDP 260 (Figure 7b). Beyond CDP 270, AVO and FVO gradients become small. AVO and FVO gradients have smooth lateral variations from small to large CDP

numbers. CDPs with the green plus in line 2 are characterized by a small increase in amplitudes with offset and a moderate frequency decay with offset (Figure 7a). In this line, both AVO and FVO gradients have small lateral variations (Figures 7b). The average AVO and FVO gradients are smaller than those in line 1. CDPs with the blue circle in line 3 show that line 3 has a wide rang of AVO gradients but is characterized by the smallest frequency variations with offset in these three lines (Figures 7a and 7b). AVO gradients in line 3 have larger lateral variations than those in line 1. In some CDPs, AVO gradients become comparable with those of line 1. FVO gradients are small and have small lateral variations. Beyond CDP 270, negative FVO gradients become large. Line 3 is characterized by its small frequency variation with offset in the attribute space.

Images from FMS logs and wellbore ellipticity analyses indicate the existence of fractures in this region. The P-S converted wave data collected in this area exhibit significant azimuthal anisotropy in the form of travel time a nd amplitude differences on the S1 and S2 shear components which are interpreted to be fracture effects (Ata and Michelena, 1995). If the azimuthal variations in AVO and FVO gradients can be attributed to the effects of fractures, the three lines have different orientations relative to the principal orientation of fractures.

To relate clusters of AVO and FVO attributes to fracture interpretation, insight into P-wave azimuthal AVO variations is obtained by using an approximation reflection coefficient equation (Ruger, 1998). Elastic parameters are obtained based on sonic and density logs acquired from well 17. We also consider the Vp/Vs estimation from the processing of P-S converted wave data. Ata and Michelena (1995) find that an average Vp/Vs ratio of 2.5 yields well focused P-S sections above and below the target zone. Saturated fluid contents are expected to be water and oil in the reservoir. The API number of crude oil (American Petroleum Institute oil gravity) is 28 (Perez, 1997). Oil density and modulus are calculated based on Batzle and Wang (1992). Anisotropic parameters were derived from Hudson's crack model (Hudson, 1981; Hudson *et al.*, 1996) and Tsvankin's expressions (1996, 1997). The parameters used in the calculation are summarized in Table 1.

Our results show that the reflection coefficient increases rapidly after intermediate incident angles. Within intermediate incident angles, the reflection coefficient has small variations with offset. Our results also show that reflection open fractures can give rise to larger amplitude increase with offset in the fracture normal direction than in the fracture strike direction. Scattering studies show that the frequency has larger decay in the crack normal direction than in the crack strike direction (Shen and Toksoz, 1998). Therefore, based on AVO and FVO characteristics, line 1 is the line most perpendicular to the principal orientation of fractures, and line 3 is the one most parallel to the principal fracture orientation. Since the properties of offset-dependent attributes in line 2 are close to those of line 1, it should be close to perpendicular to the principal fracture orientation. This interpretation is consistent with previous studies using different data sets. Borehole ellipticity analyses indicate that the direction of the present maximum

Table 1: Fracture parameters, elastic parameters, and anisotropic parameters used in analytic calculations.

Parameters	Shale	Carbonate
Vp (m/s)	3463	5150
Vs (ms)	1850	2300
ρ (g/cm^3)	2.48	2.62
Fracture density		10%
Fracture aspect ratio		0.01
$\epsilon^{(v)}$ (API28)		-0.040
$\gamma^{(v)}$ (API28)		-0.097
λ (API28)		0.107
$\epsilon^{(v)}$ (water)		-0.090
$\gamma^{(v)}$ (water)		-0.090
λ (water)		0.107
Poisson's ratio	0.300	0.375

regional stress is roughly parallel to line 3. Generally, open fractures tend to be aligned with this direction. Ata and Michelena (1995) use P-SV converted data to estimate fracture orientation and map fracture density in this area. Their studies, correlated with well data, show that fracture orientations tend to run subparallel to the fault systems and are parallel or subparallel to line 3.

EFFECTS OF BACKGROUND PROPERTIES ON AVO SIGNATURES

Effects of Fractures on AVO Signatures

Studies show that azimuthal AVO variations in fractured reservoirs are influenced by fracture parameters including fracture density, fluid content and fracture aspect ratio. In Maporal field member 'O', the material filling the crack system is expected to be oil and water. We also calculate azimuthal AVO response in the light oil (API65) saturated, fractured reservoir. Figures 8a, 8b and 8c show that, in the crack normal direction, the P-wave AVO responses vary with crack density at the top of oil- and water-saturated, fractured reservoirs. Background elastic parameters are taken from Table 1. Fractures have little effect on P-wave reflectivity except for on the intermediate incident angles. As crack density increases, the magnitudes of AVO gradients also increase. By comparing Figures 8a, 8b and 8c, we find that, with equal fracture density, water-saturated, fractured reservoirs have larger AVO gradients than oil-saturated, fractured reservoirs. However, the difference in AVO gradients between water and oil is very small. For example, for the reservoirs with 10% crack density, 0.01 fracture aspect ratio and filled by light oil (API65) and water, the difference in azimuthal AVO variations is only

2% in the crack normal direction for a 30° incident angle. Therefore, although fracture density and fluid content influence AVO signatures in off-strike fracture directions, our calculations show that the liquid content has a small influence on AVO gradients in our model.

Effects of Reservoir Heterogeneity on AVO Signatures

An important nonfracture factor influencing the azimuthal AVO variations is reservoir elastic properties, including average Vp, Vs and ρ and their contrasts. As mentioned above, near-middle offset amplitudes are most related to P-wave lithological properties of reservoirs and far-offset amplitudes contain more information about fractures than near-middle offset amplitudes. To investigate the effects of reservoir heterogeneity, caused by fluid content and porosity, on far-offset azimuthal AVO gradients and understand the large variations of AVO gradients occurring in line 3, we invert the interval velocities from near-middle offset, far-offset and the whole range of offset poststack amplitudes. In offset-dependent velocity inversion, the reflection coefficients and wavelets are also the function of offset. In line 1, velocities inverted from near-middle offset poststack amplitudes in the reservoir member 'O' gradually decrease from low to high CDP numbers and have smooth lateral variations (Figure 9a). Velocities inverted from overall poststack amplitudes have different lateral variation patterns and peak velocities distribute around CDP 250 (Figure 9b). The difference in interval velocities between Figures 9a and 9b indicates that lateral variations of near-middle offset and far-offset postack amplitudes are different from each other and that the far-offset amplitudes have a large contribution to near-middle offset amplitudes. We also note that lateral velocity variations inverted from overall poststack amplitudes are consistent with those of AVO gradients estimated in the far-offset reflections. In line 2, velocities from near-middle offset and overall poststack amplitudes are comparable with each other (Figure 10). Both of them have small lateral variations in velocities and relatively high velocities distributed between CDP 236 and CDP 260. The comparable lateral velocity variations inverted from near-middle offset and overall poststack amplitudes result from small AVO gradients and their small lateral variations in far-offset reflection. Interval velocities from near-middle offset, poststack amplitudes in line 3 show strong lateral heterogeneity in reservoirs (Figure 11a). Velocities inverted from overall poststack amplitudes have comparable lateral variation patterns (Figure 11b). Large velocities distribute along ranges in both low and high CDP numbers, from 200 to 228 and from 264 to 300. The lateral discontinuity of velocities inverted from overall poststack amplitudes still can be observed between CDP 230 and 276. The lateral variation of AVO gradients estimated from far-offset amplitudes is consistent with this lateral velocity variation. Because line 3 is parallel to the principal orientation of fractures, the AVO gradients in far-offset amplitudes are directly related to reservoir lithological properties.

By using the fracture parameters, including fracture density, fracture aspect ratio, fluid content and elastic parameters in the Table 1, our calculation from the approx-

velocities in the reservoir layer can lead to large variations of AVO gradients both in the crack normal and in the crack strike directions for a 30° incident angle. We assume that Vp of background reservoir rocks vary m/s around mean velocity 5150 m/s and that Vp/Vs is kept constant. Fractures are light oil (API65) saturated. One-dimensional synthetic P-wave velocity profile is generated by 1-D stochastic simulation. Figure 12a shows that with the increase of Vp (constant Vp/Vs), the differences of reflection coefficients between the normal incidence and 30° incidence decrease. Therefore, the AVO gradients decrease. However, the differences of reflection coefficients between the crack normal and strike directions at 30o incidence are almost the same. Furthermore, we assume that Vp of background reservoir rocks varies by 350 m/s around the mean velocity of 5150 m/s and that Vs is kept constant, hence Vp/Vs changes. The same calculations are made, and the results show that varying Vp/Vs leads to large differences of reflection coefficients between the normal incidence and 30° incidence, and the AVO gradient reverses from decreasing with offset to increasing with offset (Figure 12b). The results also show that azimuthal differences of reflection coefficients at 30° incidence decrease with increasing Vp or Vp/Vs. These calculations show that reservoir heterogeneity would have an important effect on AVO gradients even in the crack strike direction. Moreover, varying Vp and Vp/Vs simultaneously in the reservoir layer has a greater effect on azimuthal AVO variations than varying Vp and Vs (constant Vp/Vs) at the same time. Therefore, the reservoir lateral heterogeneity can be one of the major contributions to the wide range of AVO gradients in line 3. The AVO signatures are not necessarily correlated with fracture parameters, and reservoir heterogeneity has an important effect on AVO gradients.

Based on our inverted offset-dependent velocities, we would like to point out that the lithological heterogeneity in reservoirs directly influences the azimuthal offset-dependent attributes. In order to show the reservoir's spatially heterogeneous characteristics, we calculated average velocities in the reservoir layer. Figure 13a shows the distribution of CDPs of three lines in near-and far-offset velocity attribute space. Line 1 and line 2 have similar near-offset P-wave velocities and are different in far-offset velocities. Line 3 is different from line 1 and line 2 in the near-offset P-wave velocities, while it has a wide range of distribution in the far-offset velocities. In the near-offset velocity versus full range of offset velocity attribute space, line 1 and line 2 show similar properties (Figure 13b). The characteristics of azimuthal offset-dependent velocity indicate the reservoir lithological heterogeneity. The reservoir heterogeneity cannot be neglected when we use azimuthal AVO signatures to characterize the fractured reservoirs.

DISCUSSION AND CONCLUSIONS

We have demonstrated that AVO and FVO attributes estimated from seismic waveforms can be used to detect the possible principal orientation of fracture systems in reservoirs with tuning thicknesses. Moreover, estimation based on waveforms can decrease the errors caused by residual velocity and inaccurate static correction. Statistical analysis

errors caused by residual velocity and inaccurate static correction. Statistical analysis in the attribute space is very helpful for identifying major characteristics of estimated attributes, particularly when the number of wells is limited and it is not possible to carry out quantitative calibrations. Offset-dependent attributes can be selected based on their capability of providing significant statistical relationships with the fracture information. Our results show that the CDPs in line 1 are characterized by a large increase in amplitudes with offset and large frequency decay with offset and that the CDPs in line 3 are characterized by a wide variation of AVO gradients and small frequency variations with offset. Line 2 is characterized by a moderate frequency decay with offset and smaller AVO gradients than those in line 1. Knowledge of the amplitudes and frequency variations with offset provides a better understanding of the P-wave reflectivity and yields further information about the reservoir properties.

Model analysis studies are very important and very helpful in the interpretation of estimated, offset-dependent attributes. Based on our theoretical calculation derived from well data, the highest AVO gradient is in the crack normal direction at the top of fractured reservoirs. Previous studies show that the presence of fractures can lead to frequency decay with offset. If the azimuthal difference in AVO and FVO signatures can be attributed to the effects of fractures, line 3 is the closest to parallel or subparallel of the principal orientation of fractures, while line 1 is the closest to perpendicular to the fractures. Since the characteristics of attributes in line 2 is comparāble with those in line 1, line 2 is close to perpendicular to the fractures.

Although azimuthal AVO variations have been successfully used in fracture detection, our studies show that it is worthwhile to combine AVO analysis with FVO analysis. Both fracture parameters (fracture density, saturated fluid content and fracture aspect ratio) and non fracture parameters (Vp, Vs and Vp/Vs of background rocks) can influence AVO gradients and azimuthal AVO variations. Our calculations show that for the reservoir with 10% fracture density, the difference in AVO gradients between water- and oil-saturated reservoirs in the crack normal direction is 2% and the variations of Vp, Vs and Vp/Vs can lead to large variations in AVO gradients. Reservoir heterogeneity has an important effect on AVO signatures. Information about frequency variations with offset can help lessen the ambiguity in fracture detection.

To check the estimated results qualitatively, RMS amplitudes are calculated, and AVO gradients are obtained by straight-line fitting in windowed seismic waveforms in the time domain. The lateral variations of AVO gradients from the two estimation methods are approximately consistent for the three lines, which confirms the reliability of the frequency estimator.

Errors from estimation and physical interferences can contribute to distortion of the AVO and FVO estimates of gradients and intercepts. To check the validity of the straight-line fit and the oscillation in the amplitudes and frequency data, the mean absolute deviation from the fit lines is one criteria for measuring reliability. Studies from Ramos and Davis (1997) show that undulations in the normalized RMS amplitude data are caused by converted waves and coherent noise. Additionally, the CDPs with

very limited offset ranges have a small degree of reliability. These errors should be considered when making interpretations using estimated attributes.

ACKNOWLEDGMENTS

We acknowledge valuable help from Maria Perez of Intevep, Venezuela in our seismic data processing. We appreciate the helpful discussions with Dan Burns and Franklin Ruiz at M.I.T. We specifically thank Intevep S.A. for providing us with seismic data. We very much appreciate Beijing GeoSoft Development Inc. China National Petroleum Company for providing us with a research facility and support in our velocity inversion.

This research was supported by the Borehole Acoustics and Logging/Reservoir Delineation Consortium at M.I.T.

REFERENCES

Ata, E. and Michelena, R.J., 1995, Mapping distribution of fractures in a reservoir with P-S converted waves, *The Leading Edge, 12,* 664–676.

Batzle, M. and Wang, Z., 1992, Seismic properties of pore fluids, *Geophysics, 57,* 1396–1408.

Corrigan, D., Withers, R., Darnall, J., and Skopinski, T., 1996, Fracture mapping from azimuthal velocity analysis using 3-D surface seismic data, *66th Ann. Internat. Mtg., Soc. Expl. Geophys., Expanded Abstracts,* 1834–1837.

Hudson, J.A., 1981, Wave speeds and attenuations of elastic waves in material containing cracks, *Geophys. J. Roy. Astr. Soc., 64,* 133–150.

Hudson, J.A., Liu, E., and Crampin, S., 1996, Transmission properties of a plan fault, *Geophys. J. Int., 125,* 559–566.

Johnson, D.H. and DeGraaf, S.R., 1982, Improving the resolution of bearing in passive sonar arrays by eigenvalue analysis, *IEEE Transaction On Acoustics, Speech and Signal Processing, ASSP-30,* 638–647.

Levin, S.A., 1998, Resolution in seismic imaging: Is it all a matter of perspective?, *Geophysics, 63,* 743–749.

Lynn, H.B., Bates, C.R., Simon, K.M., and van Dok, R., 1995, The effects of azimuthal anisotropy in P-wave 3-D seismic, *65th Ann. Internat. Mtg., Soc. Expl. Geophys., Expanded Abstracts,* 723–730.

Mallick, S., Craft, K.L., Meister, L.J., and Chambers, R.E., 1998, Determination of the principal directions of azimuthal anisotropy from P-wave seismic data, *Geophysics, 63,* 692–706.

Mazzotti, A., 1991, Amplitude, phase and frequency versus offset applications, *Geophysical Prospecting, 39,* 863–886.

Neidell, N.S. and Cook, E.E., 1986, Seismic method for identifying low velocity subsurface zones, US Patent 4 571 710.

Paul, R.J., 1993, Seismic detection of overpressure and fracturing: an example from the Qaidam Basin, People's Republic of China, *Geophysics, 58,* 1532–1543.

Perez, M., 1997, Detection of fracture orientation using azimuthal variation of P-wave AVO response, M.S. thesis, M.I.T.

Perez, M. and Gibson, R., 1996, Detection of fracture orientation using azimuthal variation of P-wave AVO responses: Barinas field (Venezuela), *66th Ann. Internat. Mtg., Soc. Expl. Geophys., Expanded Abstracts,* 1353–1356.

Ramos, A.C.B. and Davis, T.L., 1997, 3-D AVO analysis and modeling applied to fracture detection in coalbed methane reservoirs, *Geophysics, 62,* 1683–1695.

Ruger, A., 1998, Variation of P-wave reflectivity with offset and azimuth in anisotropic media, *Geophysics, 63,* 935–947.

Schmidt, R., 1986, Multiple emitter location and signal parameter estimation, *IEEE Transaction on Antennas and Propagation, AP-34,* 276–280.

Shen, F. and Toksoz, M.N., 1998, Scattering characteristics in heterogeneous fractured

reservoirs from waveform estimation, *68th Ann. Internat. Mtg., Soc. Expl. Geophys., Expanded Abstracts,* 1636–1639.

Tsvankin, I., 1996, P-wave signatures and notation for transversely isotropic media: An overview, *Geophysics, 61,* 467–483.

Tsvankin, I., 1997, Reflection moveout and parameter estimation for horizontal transverse isotropy, *Geophysics, 62,* 614–629.

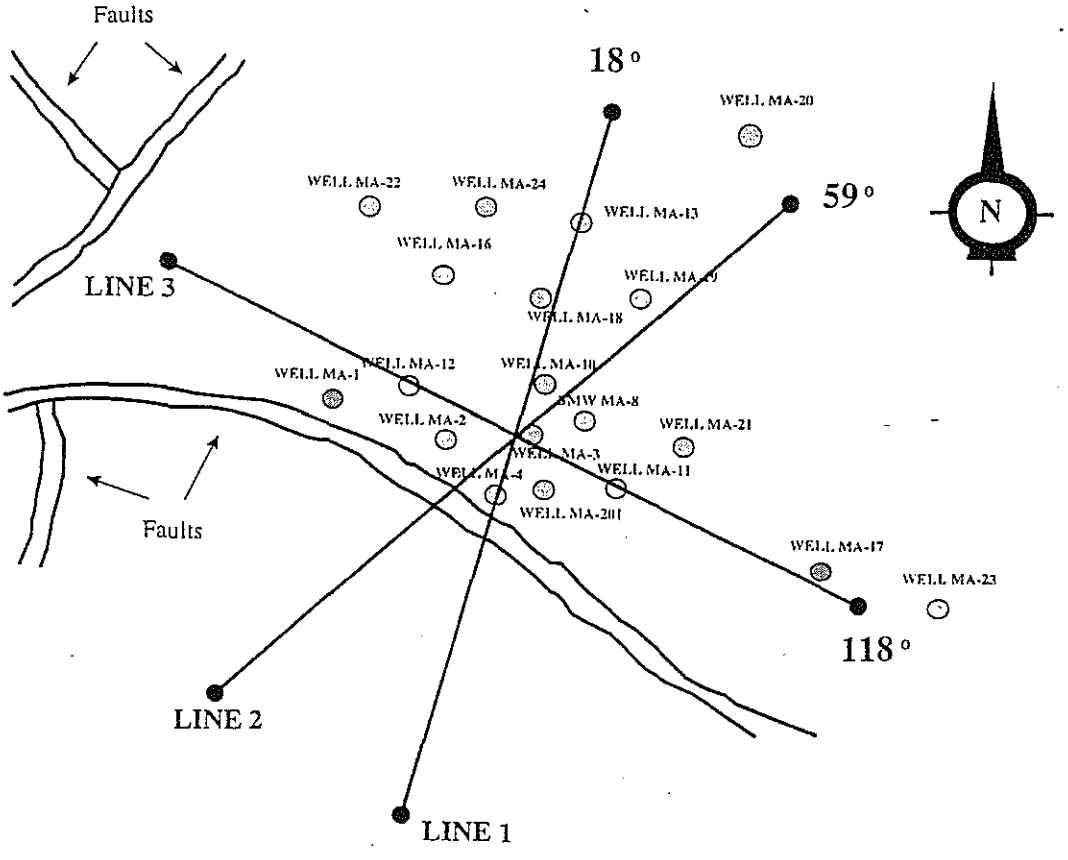

Figure 1: Locations of wells and two fault systems and geometry for three seismic survey lines in the Maporal field in the Barinas basin in southwestern Venezuela.

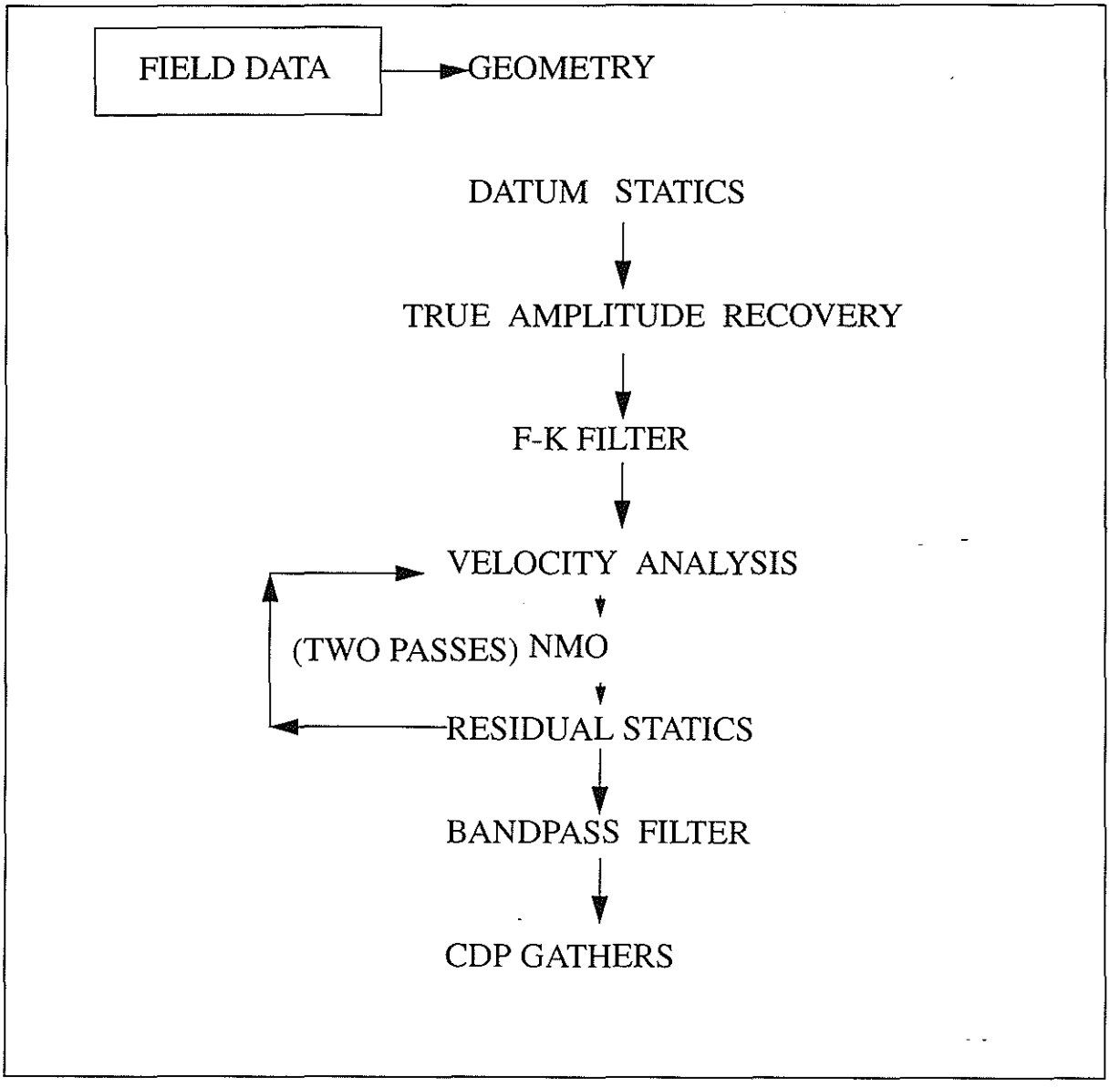

Figure 2: Data processing sequence used to obtain the prestack CDP gathers.

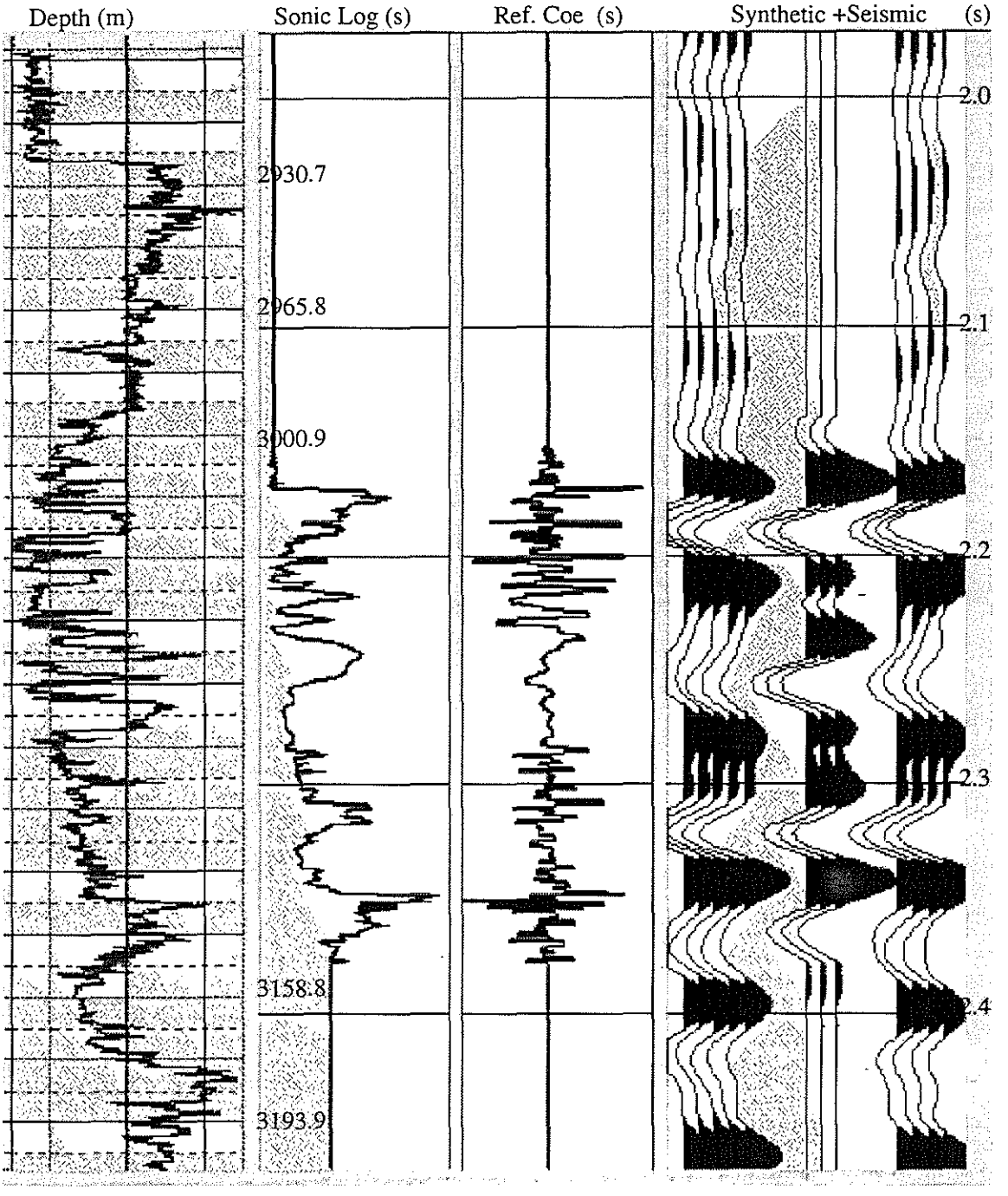

Figure 3: Tying the P-wave section of line 1 to synthetic seismograms generated from sonic logs of well 13.

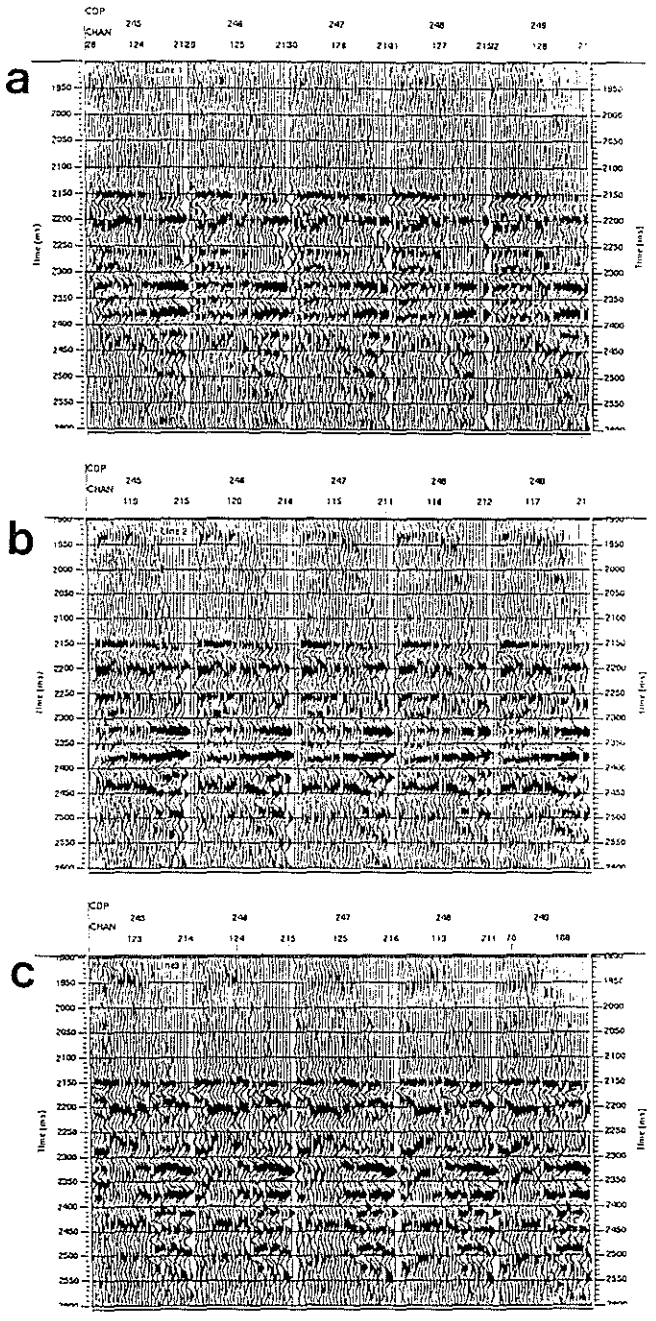

Figure 4: Prestack CDP gathers (a) CDP 245 to 249 in line 1; (b) CDP 245 to 249 in line 2; (c) CDP 245 to 249 in line 3.

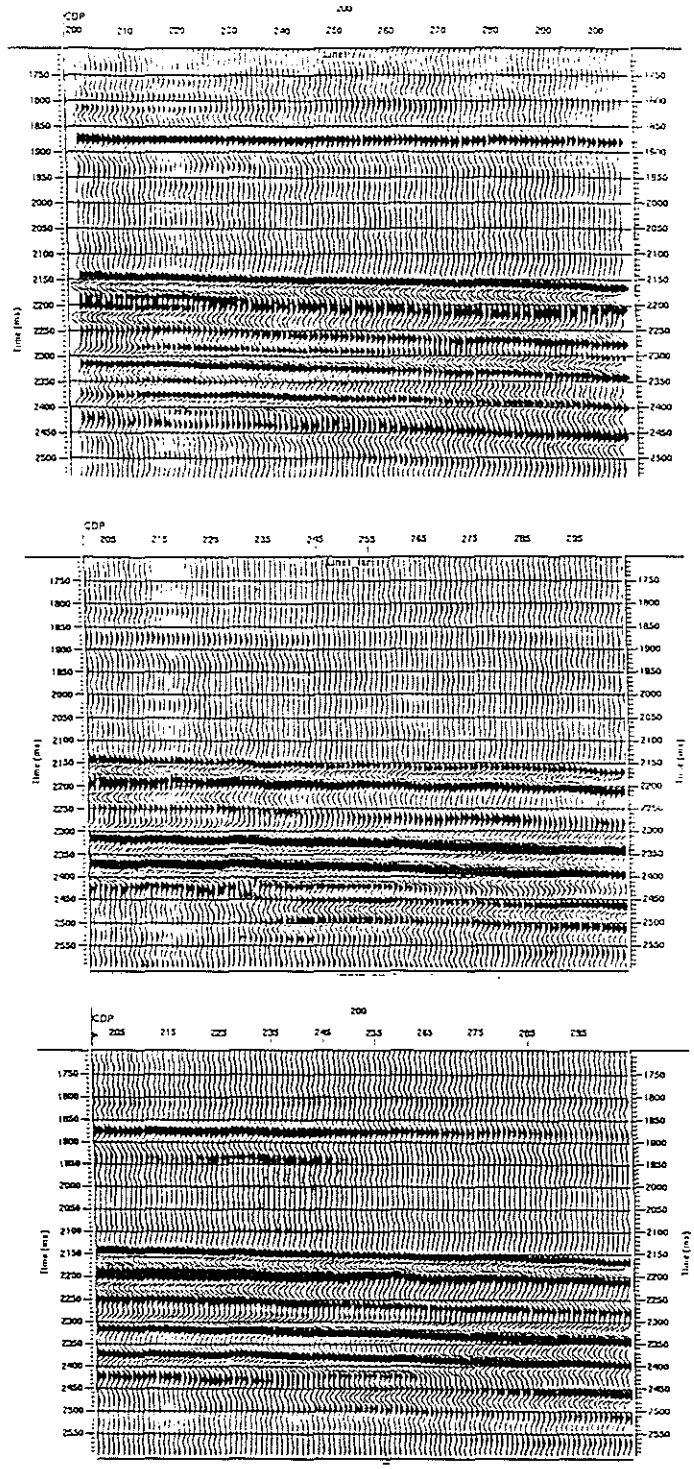

Figure 5: Five Offset-dependent poststack seismic profiles. (a) Near-middle offset, far offset and full offset poststack sections in line 1.

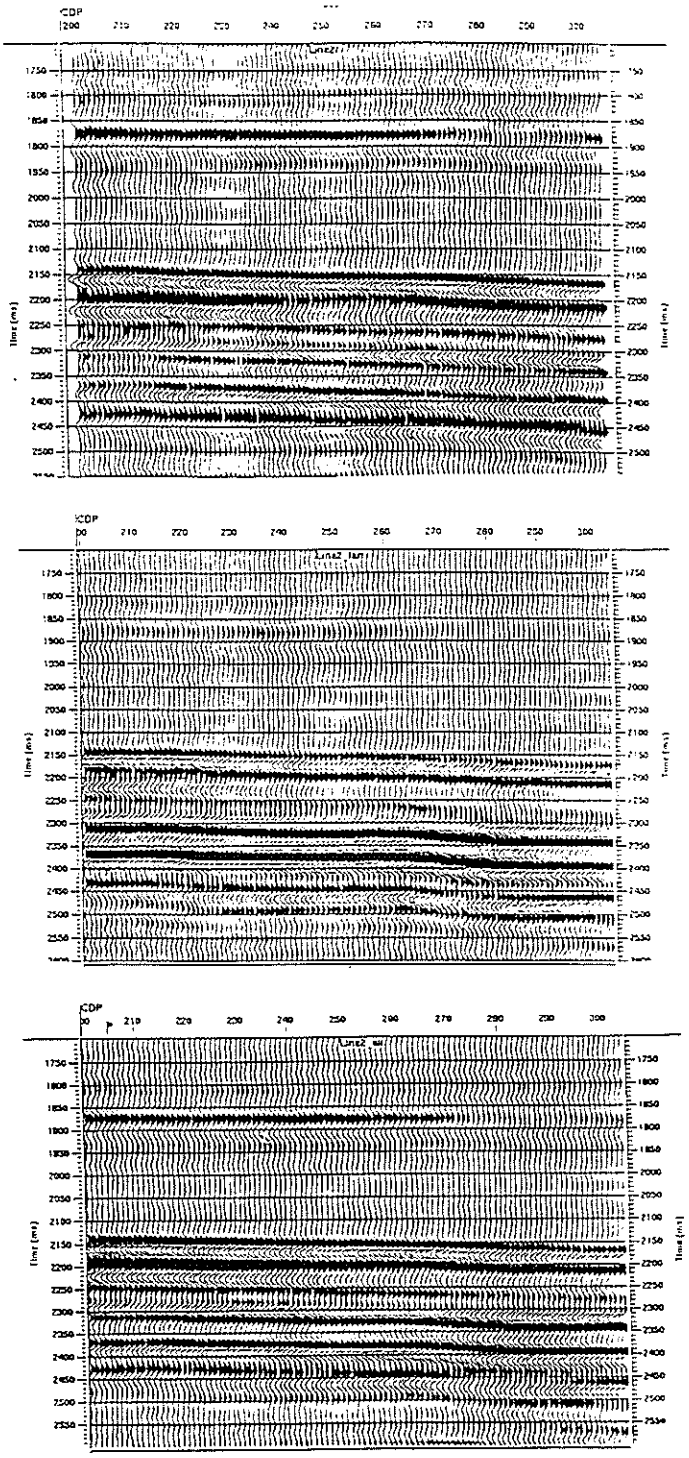

Figure 5, continued: (b) Near-middle offset, far offset and full offset poststack sections in line 2.

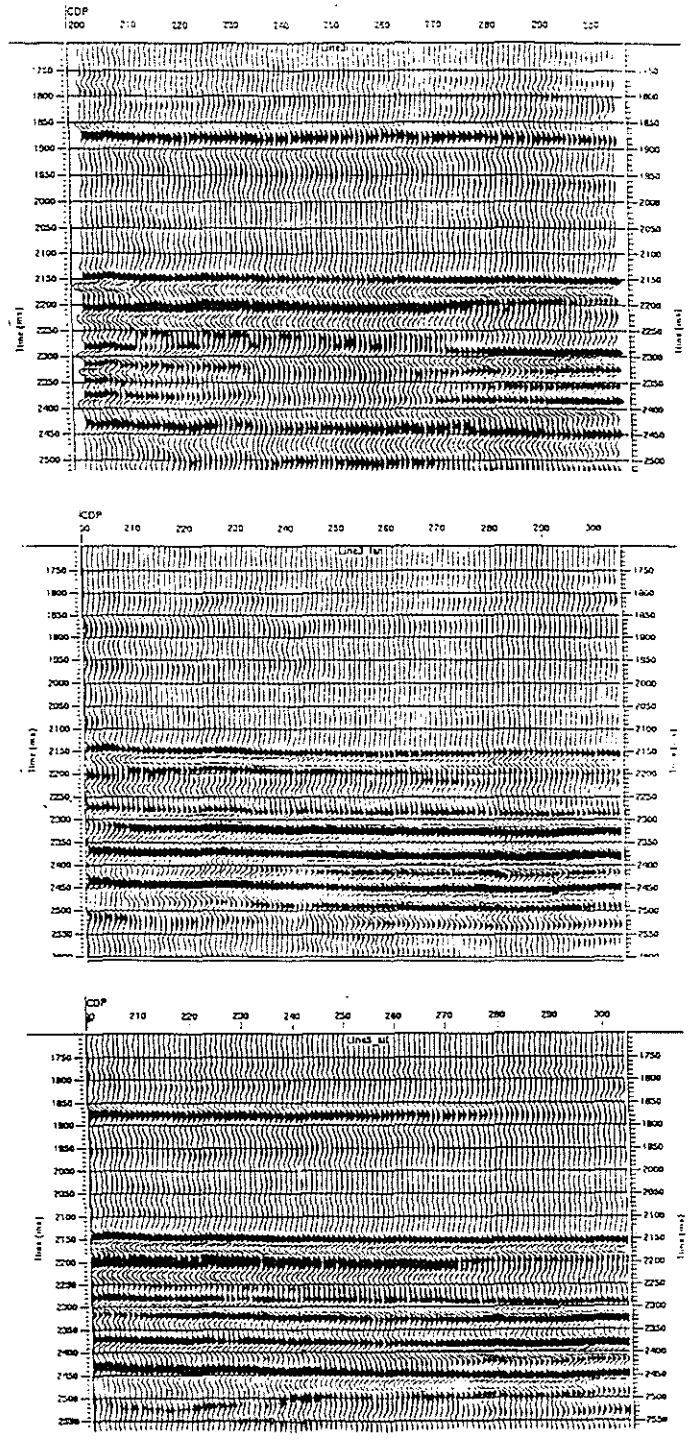

Figure 5, continued: (c) Near-middle offset, far offset and full offset poststack sections in line 3.

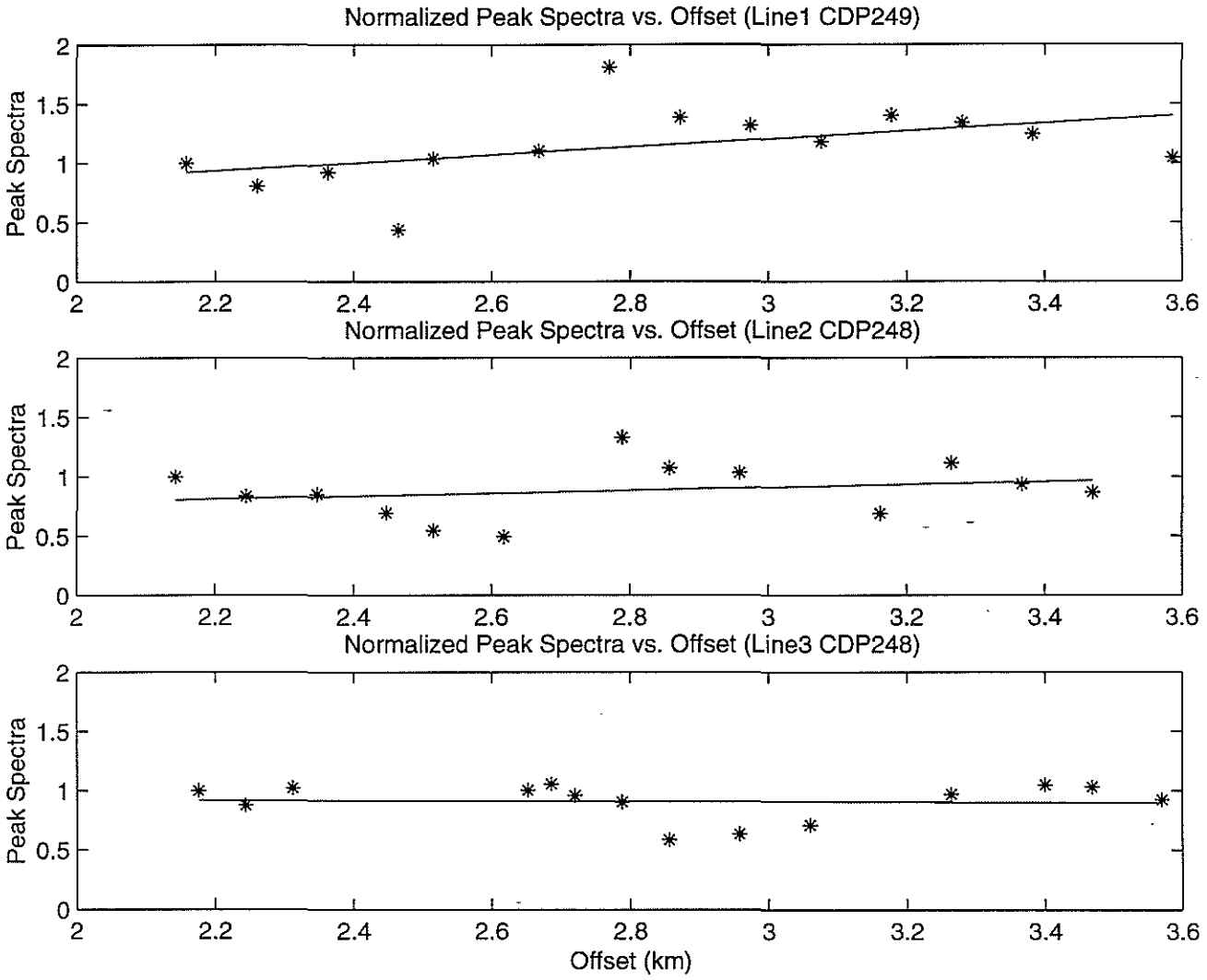

Figure 6a: Estimated normalized peak spectra versus offset at CDP 249 (line 1), at CDP 248 (line 2) and at CDP 248 (line 3).

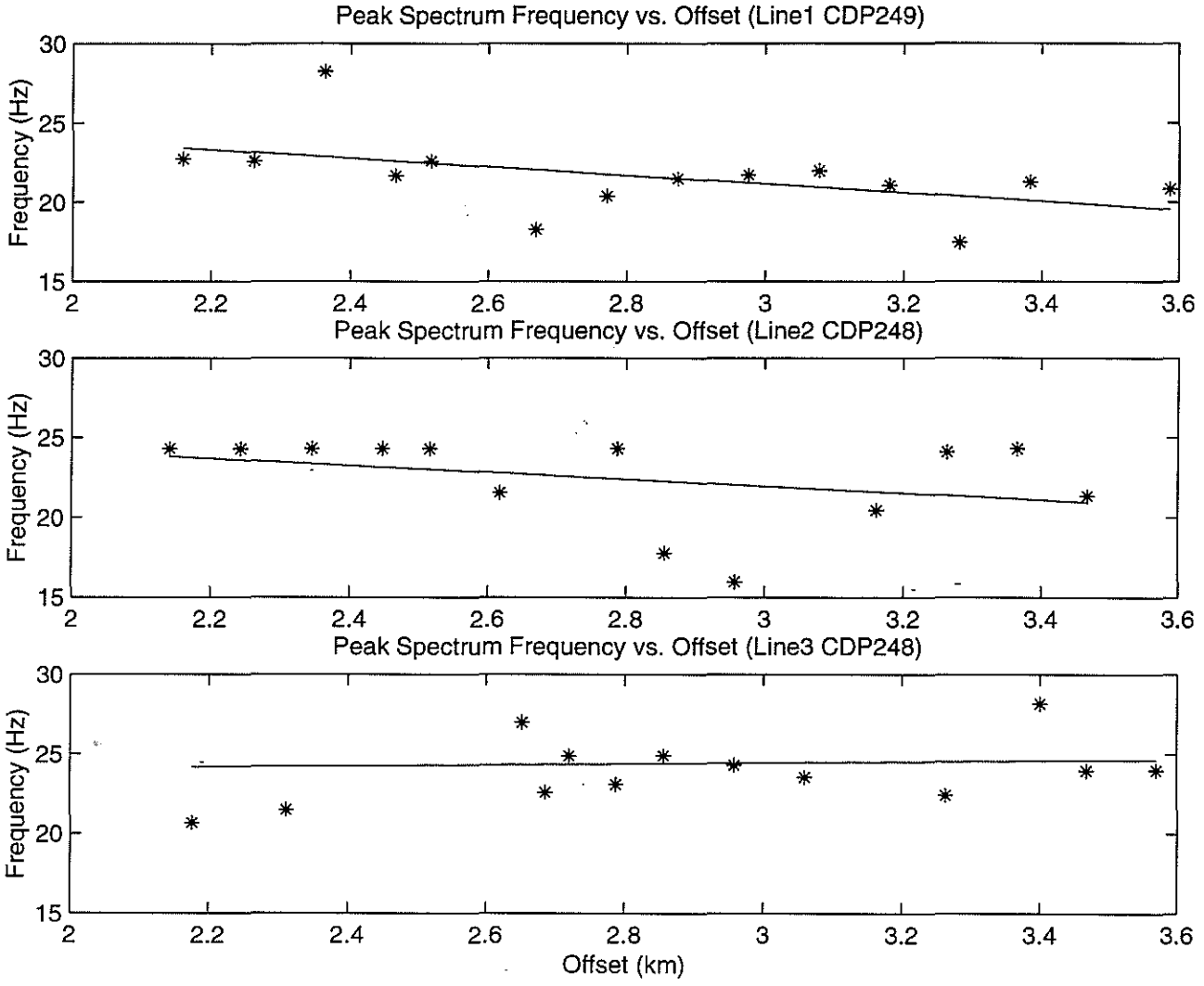

Figure 6b: Estimated normalized peak spectrum frequencies versus offset at CDP 249 (line 1), at CDP 248 (line 2) and at CDP 248 (line 3).

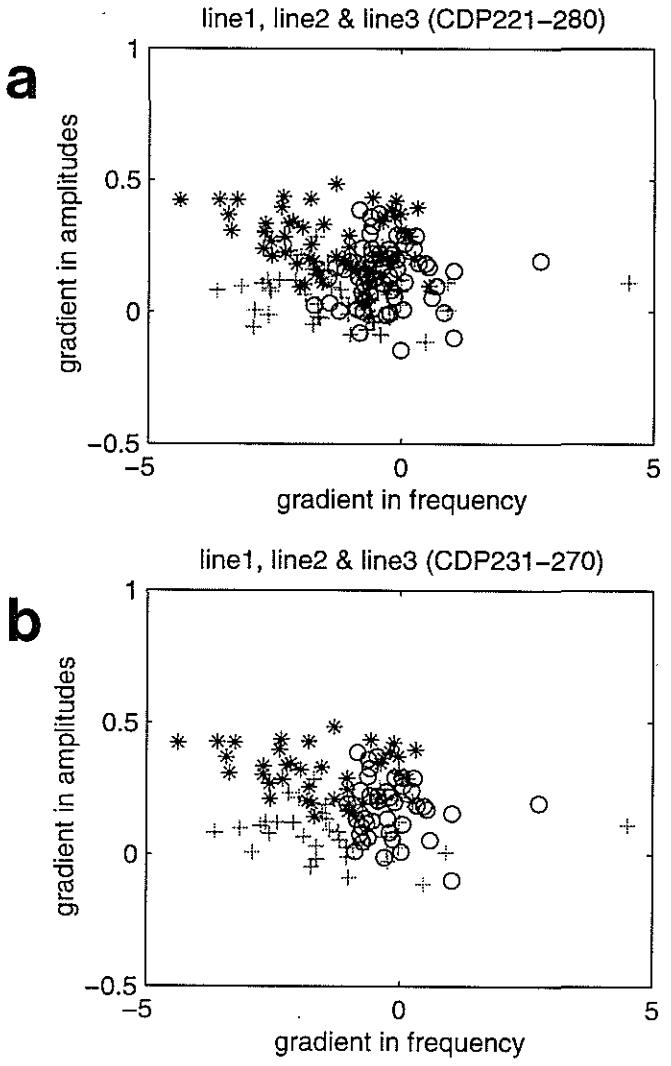

Figure 7: (a) Distributions of CDPs (221–280) in AVO and FVO gradient attribute space. ∗: CDPs from line 1; +: CDPs from line2; o: CDPs from line 3. (b) Distributions of CDPs (230–270) in AVO and FVO gradient attribute space. ∗: CDPs from line 1; +: CDPs from line2; o: CDPs from line 3.

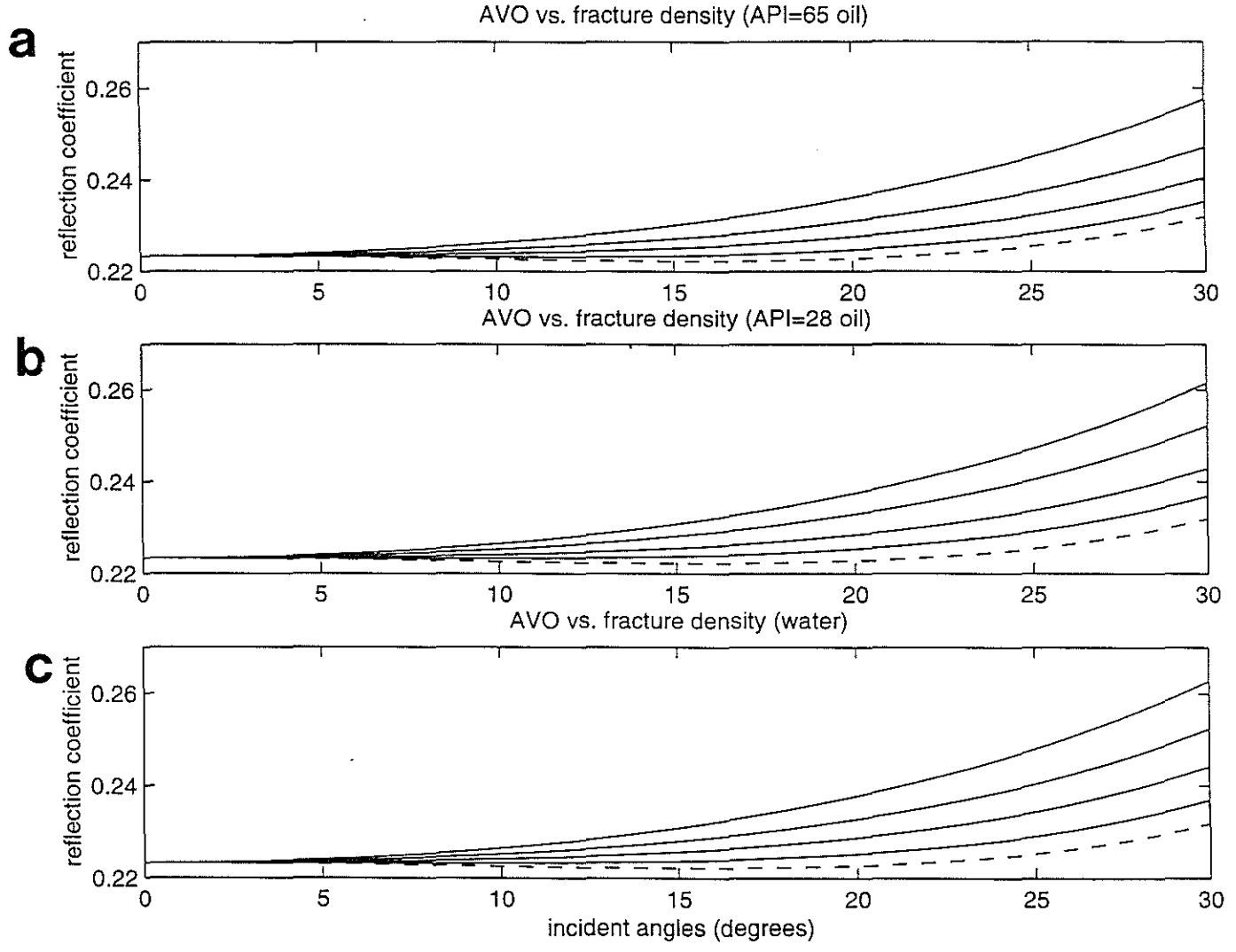

Figure 8: Theoretical calculations from parameters listed in Table 1. (a) AVO curves in light oil (API65) saturated, fractured reservoirs with fracture density 0%, 5%, 10%, 15% and 20% (from the bottom to the top). (b) AVO curves in light oil (API28) saturated, fractured reservoirs with fracture density 0%, 5%, 10%, 15% and 20% (from the bottom to the top). (c) AVO curves in water saturated, fractured reservoirs with fracture density 0%, 5%, 10%, 15% and 20% (from the bottom to the top).

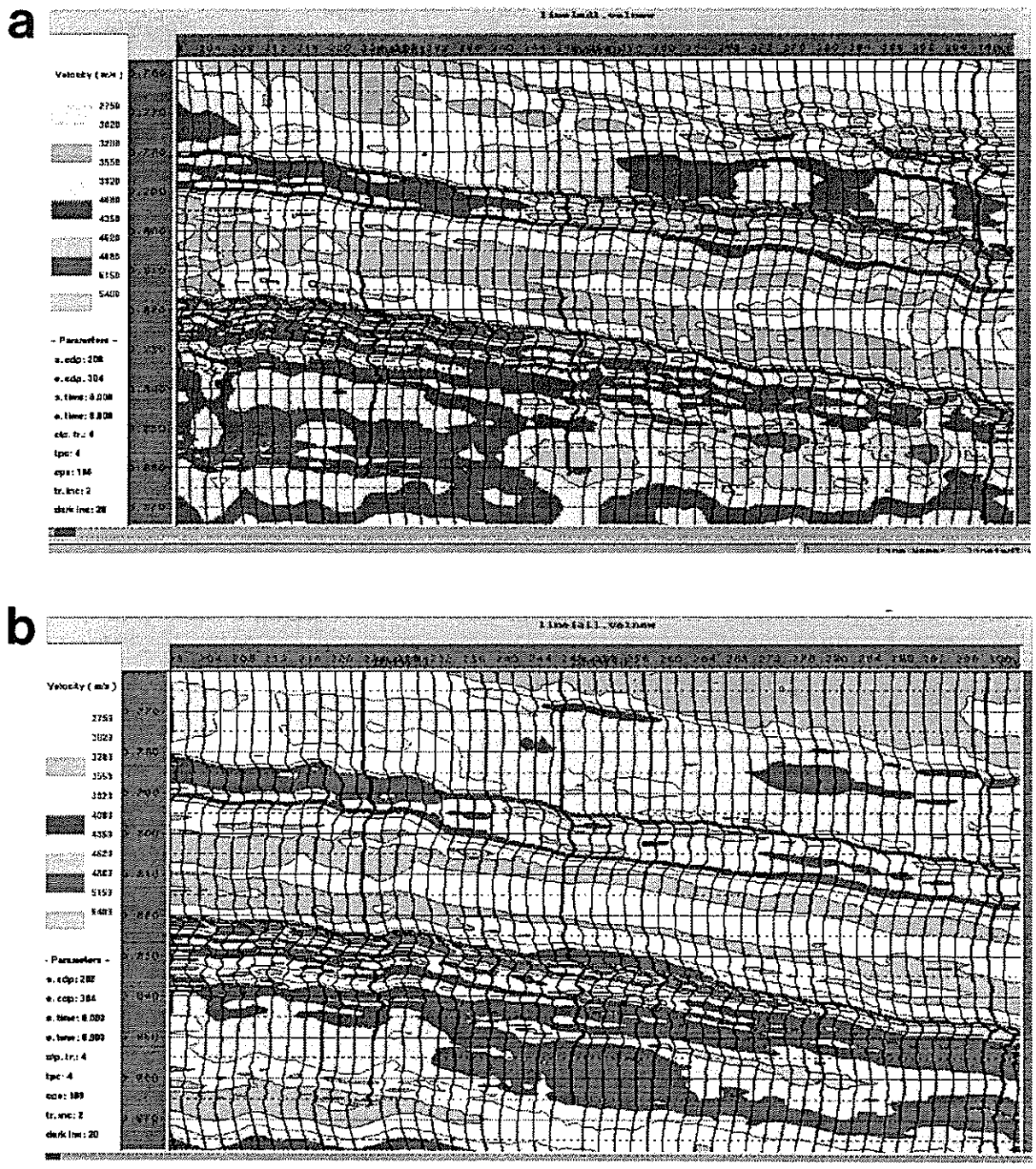

Figure 9: (a) Inverted interval P-wave velocities from near-middle poststack amplitudes in line 1. Travel time has been shifted 1.500 s. (b) Inverted interval P-wave velocities from overall poststack amplitudes in line 1. Travel time has been shifted 1.500 s.

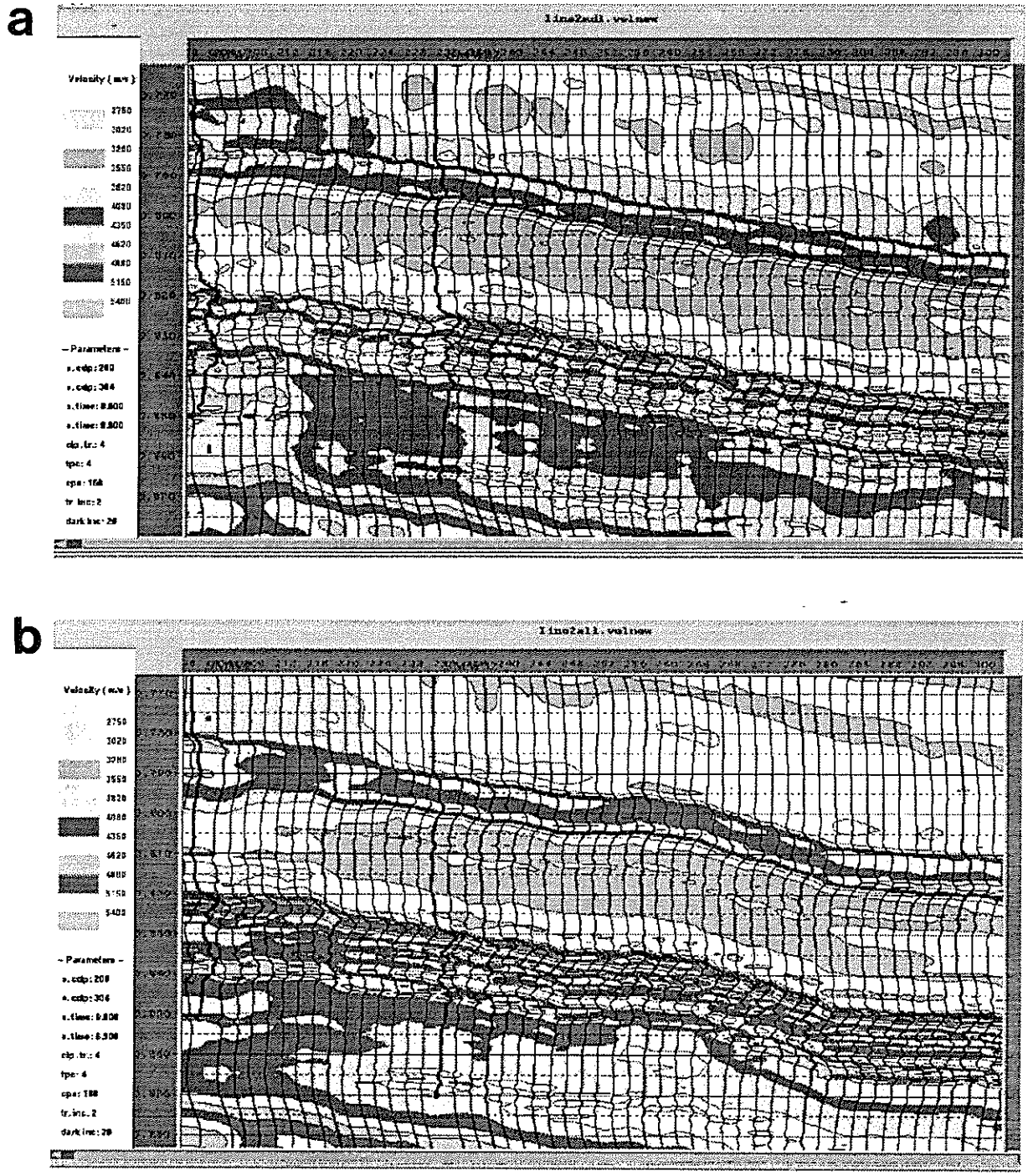

Figure 10: (a) Inverted interval P-wave velocities from near-middle poststack data in line 2. Travel time has been shifted 1.500 s. (b) Inverted interval P-wave velocities from overall poststack data in line 2. Travel time has been shifted 1.500 s.

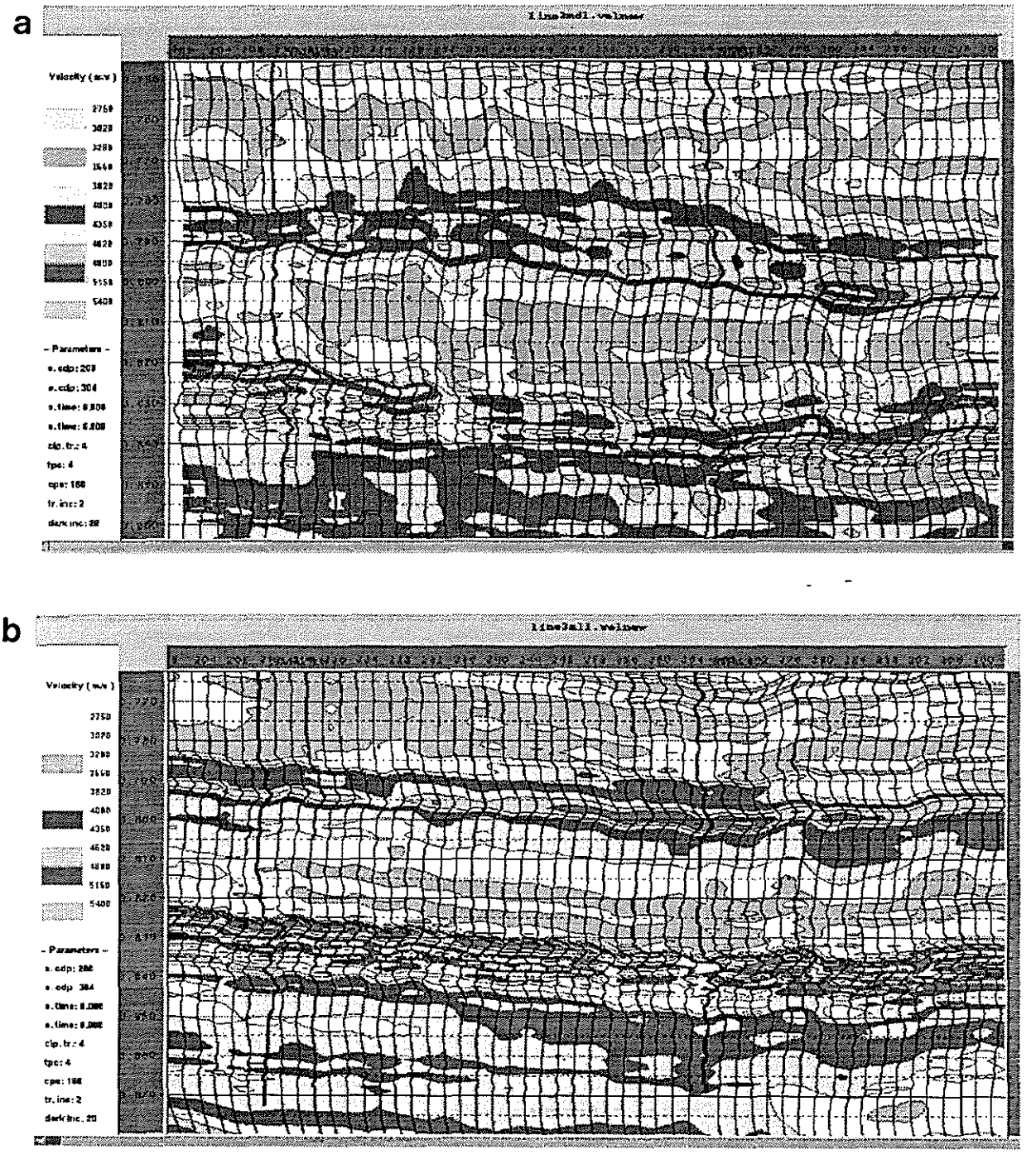

Figure 11: (a) Inverted interval P-wave velocities from near-middle poststack amplitudes in line 3. Travel time has been shifted 1.500 s. (b) Inverted interval P-wave velocities from overall poststack amplitudes in line 3. Travel time has been shifted 1.500 s.

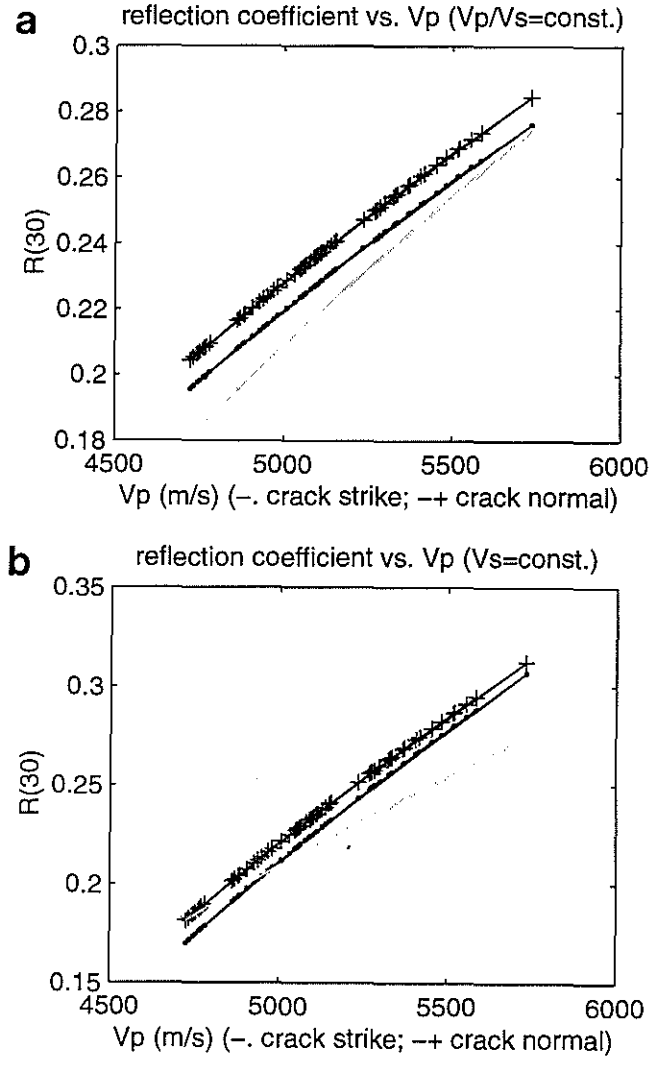

Figure 12: (a) Reflection coefficients as a function of P-wave velocities with constant Vp/Vs. Solid line: reflection coefficients at 0o incidence as a reference; solid line with dot: reflection coefficients at 30° incidence in the fracture strike direction; solid line with plus: reflection coefficients at 30° incidence in the fracture normal direction. (b) Reflection coefficients as a function of P-wave velocities with variable Vp/Vs (constant Vs). Solid line: reflection coefficients at 0° incidence as a reference; solid line with dot: reflection coefficients at 30° incidence in the fracture strike direction; solid line with plus: reflection coefficients at 30° incidence in the fracture normal direction.

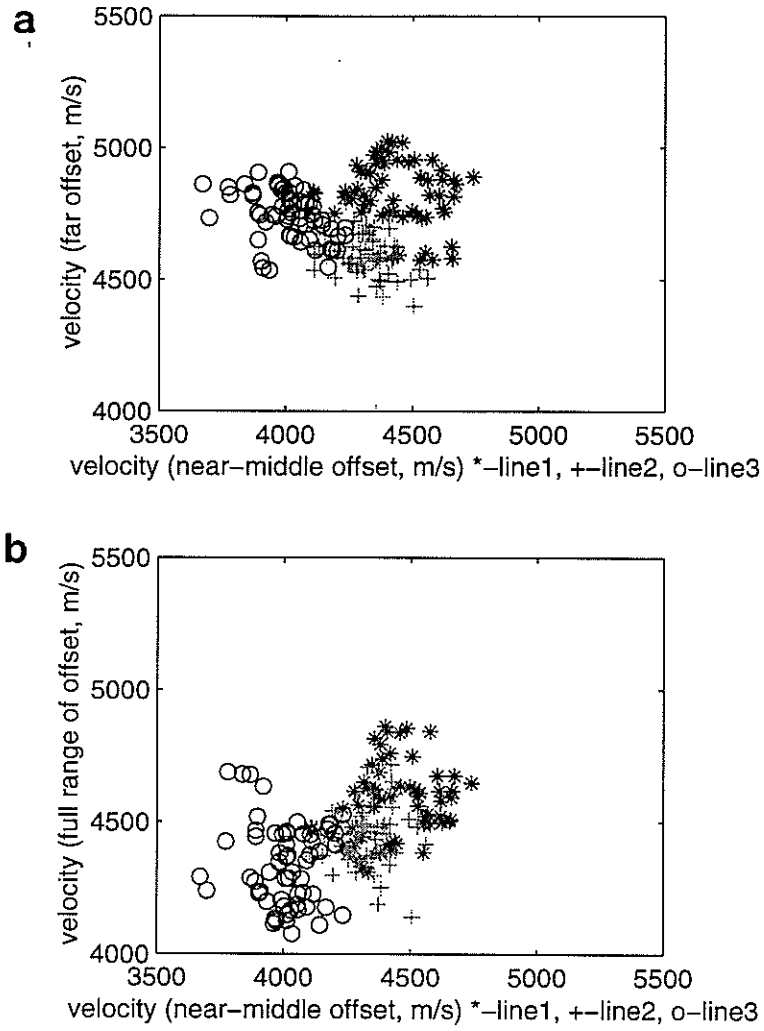

Figure 13: (a) Distributions of CDPs (221–280) in near-middle offset velocity versus far-offset velocity attribute space. $*$: CDPs from line 1; $+$: CDPs from line2; o: CDPs from line 3. (b) Distributions of CDPs (221–280) in near-middle offset velocity versus full range of offset velocity attribute space. $*$: CDPs from line 1; $+$: CDPs from line2; o: CDPs from line 3.